Progress In Electromagnetics Research C, Vol. 81, 77–88, 2018

Development of a Low Profile Wide-Bandwidth Circularly Polarized Microstrip Antenna for C-Band Airborne CP-SAR Sensor

Cahya E. Santosa[1, 2, *], Josaphat T. Sri Sumantyo[1], Katia Urata[1], Chua Ming Yam[1], Koichi Ito[3], and Steven Gao[4]

Abstract—In this paper, a low-profile wide bandwidth circularly polarized microstrip antenna is proposed as element for a C-band airborne circularly polarized synthetic aperture radar sensor. Several bandwidth improvement techniques were proposed and implemented. In order to increase impedance bandwidth, the antenna is constructed using double-stacked substrate with low dielectric constant, modified radiating shape for multi-resonant frequency, and a circle-slotted parasitic patch. Generation of the circularly polarized wave employs a simple square patch with curve corner-truncation as radiating element. The asymmetric position of the feeding is attempted to improve the axial-ratio bandwidth. To avoid a complicated feed network, the antenna is fed by single-feed proximity-coupled microstrip line. The effect of copper-covering on the upper layer for decrease undesired radiation wave emitted by the feeding is also studied and presented. Measurement results show that the impedance bandwidth and axial ratio bandwidth are 20.9% (1,100 MHz) and 4.7% (250 MHz), respectively. Meanwhile the measured gain is 7 dBic at the frequency of 5.3 GHz.

1. INTRODUCTION

Synthetic aperture radar (SAR) is an active sensor that transmits electromagnetic pulse and receives the scattering signal from an object with physical properties that allows all-weather day to night time operation. Research and development of compact SAR system are rapidly increasing with lower costs [1]. Commonly SAR sensors operate using linearly polarized electromagnetic waves [2]. However, linearly polarized electromagnetic waves are sensitive to antenna orientation mismatch, in addition to Faraday rotation effects occurring in the ionosphere, degrading the receiving signal [3, 4]. In circularly polarized synthetic aperture radar (CP-SAR) sensors, such issues can be overcome [1].

For onboard payloads, the limitations in antenna weight and dimension are the main challenges in CP-SAR sensor development. Compact sizes, lightweight, low profile, low cost, and easy fabrication of high performance antennas have become highly-desired attributes. Microstrip antenna is a potential candidate to realize the onboard CP-SAR sensor, but unfortunately, also has several limitations in antenna characteristics such as low power, low efficiency, and very narrow frequency bandwidth [5–8].

In recent years, several methods have been proposed to broaden the impedance bandwidth (IBW) and 3 dB axial ratio bandwidth (ARBW) of CP antennas. Substrate selection is the first step to be considered in designing wide IBW microstrip antenna. Theoretically, a wide IBW can be reached by decreasing the Q-factor, which can be achieved by increasing the substrate thickness or decreasing the dielectric constant of the substrate [5–8]. On top of that, constructing the antenna on thick multi-layered substrates, foam, or full-air gap have also been studied; IBW obtained has shown to be

Received 9 November 2017, Accepted 23 January 2018, Scheduled 6 February 2018

* Corresponding author: Cahya Edi Santosa (cahya.edi@chiba-u.jp).

[1] Center for Environmental Remote Sensing (CEReS), Chiba University, Japan. [2] Center for Aviation Technology, National Institute of Aeronautics and Space, Bogor, Indonesia. [3] Research Center for Frontier Medical Engineering, Chiba University, Japan. [4] Department of Engineering and Digital Arts, University of Kent, Centerbury, CT2 7NZ, UK.

approximately 20–40% and ARBW around 10–25% [9–12]. However, such implementation for onboard CP-SAR sensor poses several challenges considering existing mechanical vibrations that may affect the antenna structural stability and overall performance. Other methods employing a single-feed proximity-coupled microstrip line in antenna feeding modification have been reported in [13–16] to broaden IBW. Although dual-feed technique can provide better stability of the CP wave than single-feed, the latter provides a simpler feeding and reduced fabrication costs in array configuration. IBW improvement by using a slot and perturbation techniques have also been reported [17–20]; however, the problem of low gain arises due to its bi-directional radiation pattern. Gain enhancement is compromised by limitation of mounting space available for the onboard CP-SAR sensor. Adding a parasitic patch has already been proven to broaden ARBW and to enhance the gain deficiency [21, 22]. Previous research has combined both parasitic patch and slot element to enhance ARBW [23], but the gain has not been improved significantly.

Currently, Center for Environmental and Remote Sensing (CEReS), Chiba University, Japan, is developing an L, C, and X-band airborne CP-SAR to observe disaster and environmental change. Table 1 lists the specifications required for the C-band CP-SAR sensor. Several CP-SAR sensor designs have been proposed, but the overall antenna array performance did not fulfill CP-SAR system requirements with regard to IBW and ARBW, both obtaining less than 5% [24, 25]. In order to meet these requirements, a wide bandwidth CP-SAR sensor is needed. This paper presents a new design of a single patch wide bandwidth CP microstrip antenna for C-band CP-SAR sensor. Several efforts for IBW and ARBW improvement techniques, such as stacked double-layer substrate, modified shape of parasitic patch, shifted position of feeding line, and circle-slotted parasitic patch, are then presented and discussed. The paper is organized as follows. Section 2 describes the detailed antenna design and bandwidth improvement techniques. In Section 3, the realized antenna and verification result are presented and discussed. Section 4 concludes the findings.

Table 1. Specifications of microstrip array antenna for C-band CP-SAR sensor.

Parameter	Value	Parameter	Value
Center frequency (f_c)	5.3 GHz	Total gain	> 20 dBic
Impedance bandwidth	400 MHz (7.6%)	Side-lobe level	-20 dB
3 dB ARBW	400 MHz (7.6%)	Cross-pol isolation	-20 dB
Range beam-width	10° (E-plane)	Tilt angle	25°–35°
Azimuth beam-width	5° (H-plane)	Antenna size	400 mm × 1500 mm × 10 mm

2. ANTENNA DESIGN

2.1. Geometry of the Antenna

Figure 1(a) depicts the substrate configuration of the proposed antenna. The antenna is constructed by stacking a two-layer substrate, with 1.6 mm thickness (h), dielectric constant (ϵ_r) of 2.17, copper cladding thickness (t) of 0.035 mm, and dissipation factor (tan-δ) of 0.0005. In order to broaden the IBW, the proposed antenna employs a thick substrate with low dielectric constant. For simplification in

Table 2. The dimension of the antenna.

Variable	Length (mm)	Variable	Length (mm)	Variable	Length (mm)
w_s	42.4	l_s	65.5	s_p	2.5
w_p	17.8	l_p	17.8	r_o	26.5
w_f	1.5	l_f	25.8	b_1	7.0
w_z	2.0	l_z	9.6	b_2	5.5

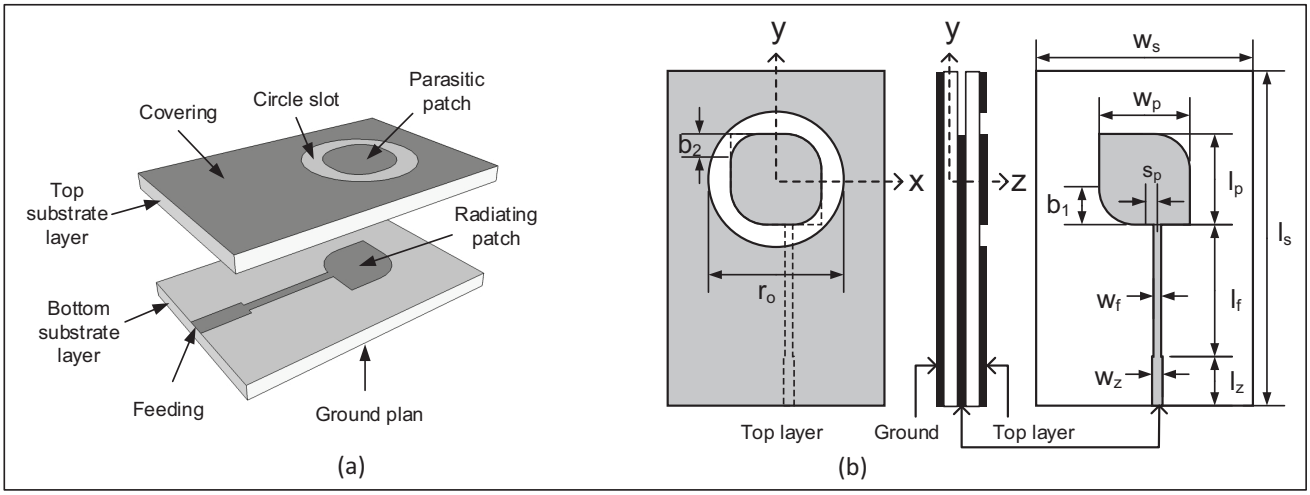

Figure 1. Configuration of the proposed antenna. (a) 3D view; (b) detailed geometry.

the antenna design, a square patch with diagonally curve corner-truncation is adopted as the radiating patch, fed by a single-feed proximity-coupled microstrip line placed in between the substrates. In the upper layer of the top substrate, a parasitic patch is placed at the center of the radiating patch in order to improve the ARBW and gain. To reduce the undesired electromagnetic field emitted by the feeding, the upper layer of the top substrate is covered by copper. The ground plane is a copper sheet placed at the bottom layer of the antenna. Detailed geometry of the proposed antenna is as illustrated in Fig. 1(b), and the dimension is listed in Table 2.

2.2. Circularly Polarized Wave Generation

A square patch with corner-truncation is adopted as radiating patch to achieve a simple design for circularly polarized wave generation [4]. The dimensions of radiating patch can be calculated by using Equations (1)–(4) [5].

$$w_p = \frac{v_o}{2f_r}\sqrt{\frac{2}{\epsilon_r+1}} \tag{1}$$

$$\epsilon_{reff} = \frac{\epsilon_r+1}{2} + \frac{\epsilon_r-1}{2}\left[1+12\frac{h}{w_p}\right]^{-1/2} \tag{2}$$

$$\frac{\Delta l_p}{h} = 0.412\frac{(\epsilon_{reff}+0.3)\left[\frac{w_p}{h}+0.264\right]}{(\epsilon_{reff}-0.258)\left[\frac{w_p}{h}+0.8\right]} \tag{3}$$

$$l_p = \frac{v_o}{2f_r\sqrt{\epsilon_{reff}}} - 2\Delta l_p \tag{4}$$

where v_o is the speed of light in vacuum, f_r the resonant frequency, ϵ_{reff} the effective dielectric constant, and Δl_p the extended incremental length of the patch antenna. For center frequency of 5.3 GHz, the width (w_p) and length (l_p) of the squared patch are calculated as 22.46 mm and 18.25 mm, respectively. The design of the antenna is optimized using Method of Moments (MoM) with the full wave simulation software CST Studio Suite 2017. Dimensions of w_p and l_p are adjusted to match those of the circularly shaped patch for ARBW enhancement. After optimization, final values for w_p and l_p of the radiating patch obtained are 17.75 mm or 20.7% lower than w_p from the calculation result.

Figure 2 shows the surface current distribution of the proposed antenna in radiating CP wave at frequency of 5.3 GHz. The pictures depict the antenna excitation at 90° phase differences in the $+z$-direction. The radiating patch areas that have dominant surface current are indicated by letters A, B,

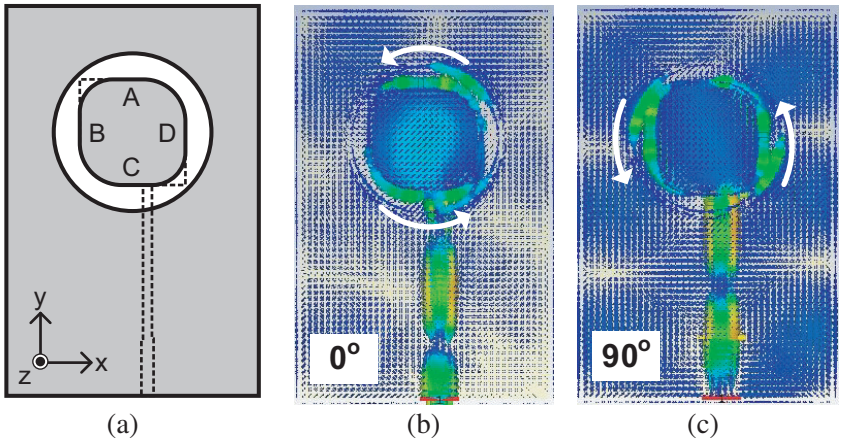

Figure 2. Surface current distribution simulation. (a) Simplified geometry of the antenna. Excitation at different time phase: (b) 0° phase; (c) 90° phase.

C and D in Fig. 2(a). Meanwhile, the flow direction of the dominant surface current is shown by white arrows in Fig. 2(b) and Fig. 2(c). When the phase is equal to 0° as illustrated in Fig. 2(b), the surface currents are concentrated at area A and area C, in which, A flow is towards $-x$-direction and C in the opposite direction. For the 90° phase, the dominant current is now concentrated at area B and area D, which creates the flow direction of area B towards $-y$-direction and in the opposite direction for area D. After 180° phase shift, the surface current distribution rotates in counter-clockwise direction generating right-handed circularly polarized (RHCP) electromagnetic waves.

2.3. Impedance and Axial Ratio Bandwidth Improvement Techniques

Several techniques are currently proposed and implemented, so that the IBW and ARBW of the designed antenna is further improved. These techniques are detailed below.

2.3.1. Multi Resonant Frequency

Figure 3 illustrates the evolution in the efforts to improve the IBW and ARBW of the designed antenna. In the first step, the antenna is constructed by using the same dimension of the radiating patch and

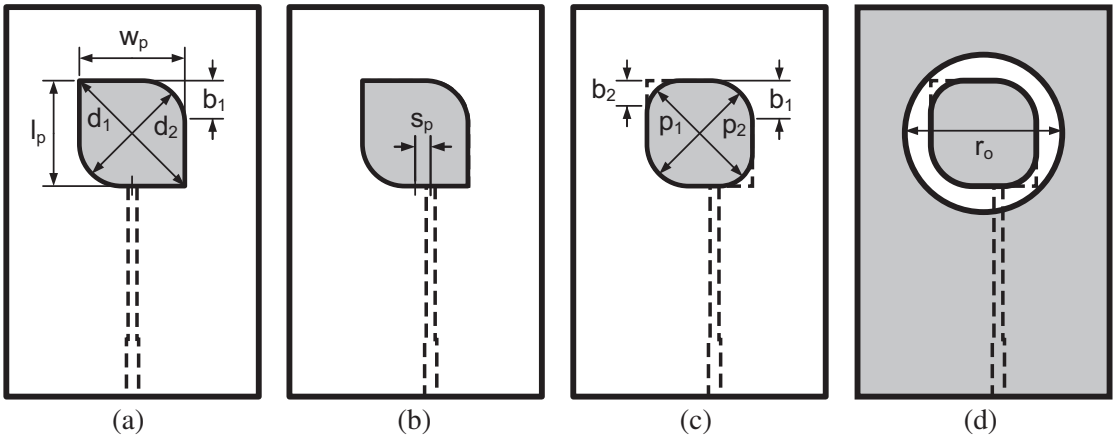

Figure 3. Evolution in the proposed antenna for bandwidth improvement (a) square patch with corner-truncation; (b) shifted position of microstrip line feeding; (c) Modified shape of parasitic patch; (d) circle-slotted parasitic patch.

parasitic patch as shown in Fig. 3(a). The square patch has left diagonal length of d_1 mm and right diagonal length of d_2 mm. The radiating patch and parasitic patch are designed to have the same curve corner-truncation (b_1) level. Any changes made on b_1 will change the right diagonal length of d_2. On the other hand, the left diagonal length d_1 is determined by the radiated patch length l_p and radiated patch width w_p. This controls the antenna's surface current distribution and optimizes the axial ratio (AR) and the resonant frequency within operational bandwidth of the antenna.

To approximate to the resonant frequency, detailed geometries of the radiating patch and parasitic patch of the antenna are described in Fig. 4(a) and Fig. 4(b), respectively. Adjustment method to calculate the corner truncation size and diagonal length of the patch are defined by Equations (5)–(10). Estimated values for d_2 and p_1 are arranged between maximum value of $w_p = 22.46$ mm and minimum value of $l_p = 18.25$ mm, which have been calculated by Equations (1)–(4) before. After optimization, the optimum IBW and ARBW of the proposed antenna are obtained with value of d_2 equal to 19.37 mm and p_1 equal to 20.61 mm, or in other words $b_1 = 7.0$ mm and $b_2 = 5.5$ mm, respectively.

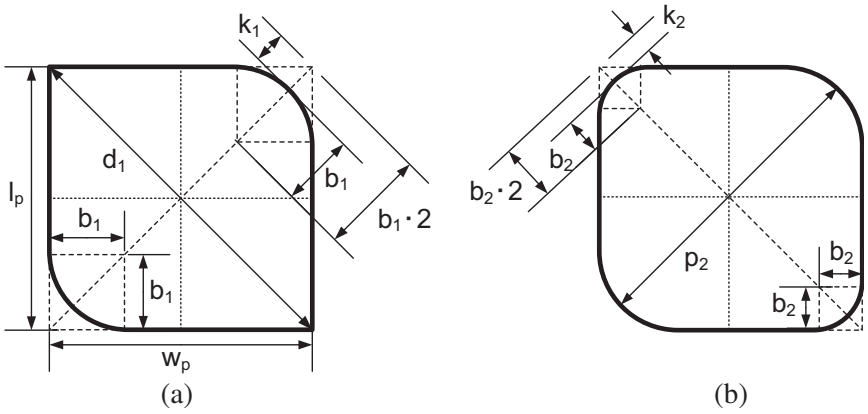

Figure 4. Detailed geometry of (a) radiating patch and (b) parasitic patch to describe the adjustment method of corner truncation size and diagonal length.

The effects in the return loss (RL) and the AR of the antenna due to the curve corner-truncation level (b_1) are shown in Fig. 5(a). The right diagonal length of the radiating patch (d_2) determines the resonant frequency and the 3 dB ARBW. A longer right diagonal length d_2 (consequently, shorter in b_1) will lower the antenna resonant frequency but increase the ARBW of the antenna. Nevertheless, a shorter right diagonal length d_2 (consequently, longer in b_1) will raise the resonant frequency of the antenna and shift the ARBW into the operational bandwidth region. By adjusting the ratio of d_1 and d_2, the resonant frequency and the ARBW are tuned to the required bandwidth and operating region.

$$d_1 = w_p\sqrt{2} = l_p\sqrt{2} \tag{5}$$

$$k_1 = b_1\sqrt{2} - b_1 \tag{6}$$

$$k_2 = b_2\sqrt{2} - b_2 \tag{7}$$

$$d_1\frac{1}{2} = \frac{1}{2}w_p\sqrt{2} - k_1 = \frac{1}{2}w_p\sqrt{2} - (b_1\sqrt{2} - b_1) \tag{8}$$

$$d_2 = p_2 = w_p\sqrt{2} - 2b_1\sqrt{2} + 2b_1 \tag{9}$$

$$p_1 = w_p\sqrt{2} - 2b_2\sqrt{2} + 2b_2 \tag{10}$$

2.3.2. Shifted Feed Line Position

For the current antenna array configuration, since pin-fed microstrip antenna may pose increased manufacturing costs, edge-fed microstrip is here considered. Fig. 3(b) illustrates the effect of the feed line position on the radiating patch, in order to investigate the optimum ARBW. Conventionally, the feed line of a microstrip patch antenna is placed at the midpoint of an edge or at the corner of the

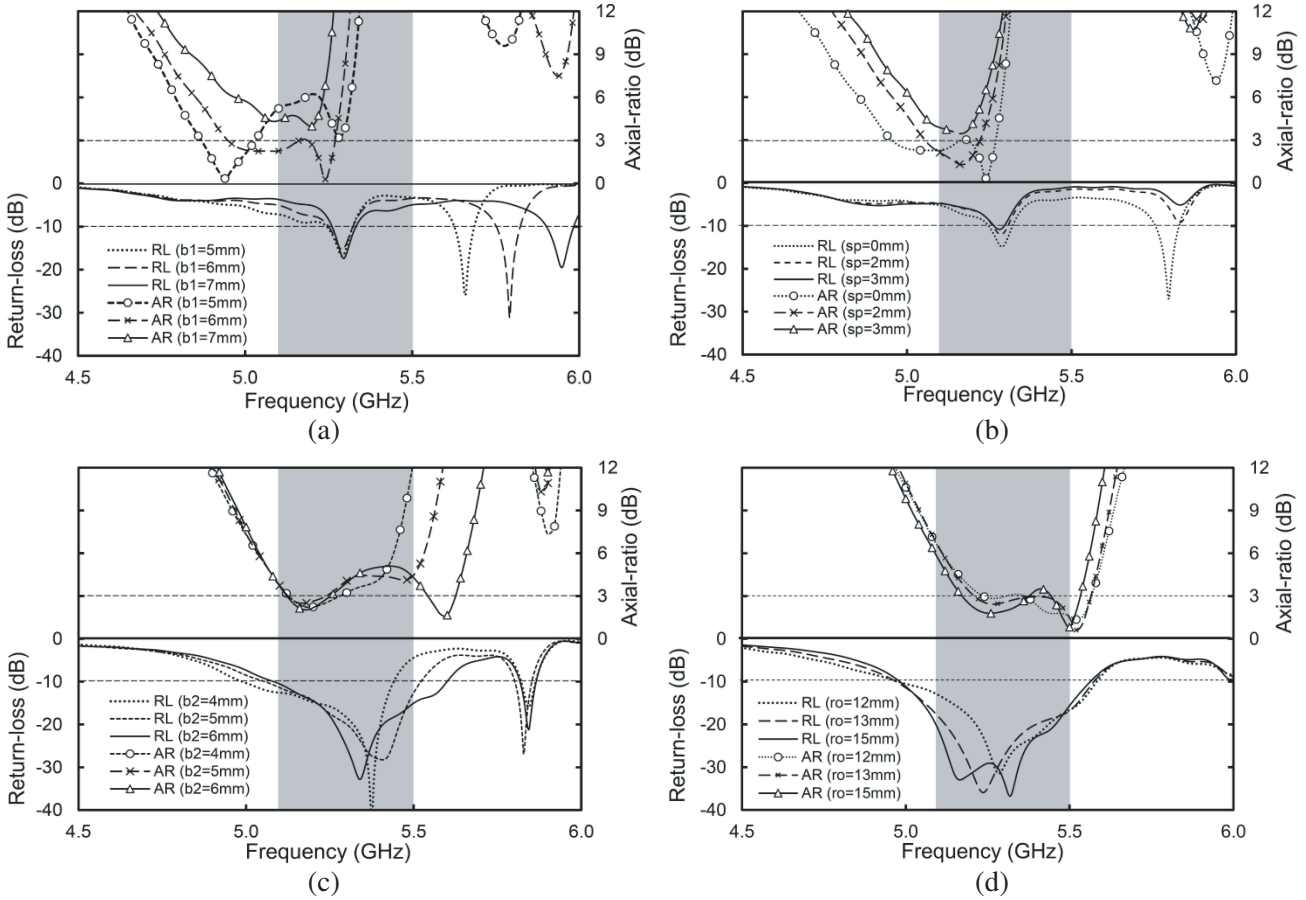

Figure 5. Simulated RL and AR of the antenna in investigating the effects of: (a) corner-truncation, b_1; (b) feed line position, s_p; (c) corner-truncation of parasitic patch, b_2; (d) diameter of circle-slotted parasitic patch, r_o.

radiating patch. In the proposed antenna design the end line position is shifted towards the tapered side of the squared patch. Shifting the position of the feed line changes the surface current flow direction distribution on the radiating patch.

The effects of shifting the feed line position towards the characteristic of IBW and ARBW of the antenna is investigated and presented in Fig. 5(b). The graph clearly shows that the entire ARBW is shifted to the desired region when the position of feed line is changed to a higher value. The ARBW is also changed as a result of the feed shifting. The optimization of feed line position enhances the performance of AR within the operational region.

2.3.3. Modified Shape of Parasitic Patch

Another technique to broaden the bandwidth and improve the AR quality is by applying a parasitic patch above the radiating patch in the top layer of the antenna. Fig. 3(c) shows the geometry of the parasitic patch with corner-truncation sizes of b_1 and b_2, and diagonal lengths of p_1 and p_2.

The bandwidth can be broadened by adding a new part in which its operating frequency is in the middle of the lowest and the highest frequencies by adjusting the value of p_1. The value of b_2 can be adjusted to direct the flow of surface current distribution of the parasitic patch for a smooth circularly polarized wave.

Figure 5(c) plots the simulated RL and AR for various values of b_2. The IBW increases in proportion to the value of b_2, but the ARBW is significantly changed. High value in b_2 leads to a circular shape in the parasitic patch.

2.3.4. Circle-Slotted of Parasitic Patch

Almost all area in top layer of the proposed antenna is covered by copper. However, a circle slot is created around the parasitic patch as illustrated in Fig. 3(d). The purpose of the copper-covering is to suppress the undesired electromagnetic radiation emission from the feeding network when the patch is placed in the array configuration. The effects of copper-covering towards the characteristics of the antenna are studied and summarized in Table 3. The table shows that circle-slotted copper-covering widens the IBW and ARBW compared to the antenna without any copper-covering. However, the tradeoff is a lower antenna gain. Copper-covering does not absorb the electromagnetic wave emitted by feeding line, and instead, part of the wave is deflected back into substrate. Unfortunately, the reflection influences the radiation pattern of the radiating patch in the antenna. Nevertheless, the simulation results of the antenna with copper-covering indicate that the 3 dB beamwidth grows wider in E-plane with the boresight of main lobe not centering at 0°, both in E-plane and H-plane.

Table 3. Characteristic of the antenna with and without the copper-covering (simulated) Note: H-BM is the H-plane beam-width; E-BM is the E-plane beam-width; H-BS is the H-plane bore-sight; and E-BS is the E-plane bore-sight.

Copper-covering	IBW (MHz)	ARBW (MHz)	Gain (dBic)	H-BM (°)	E-BM (°)	H-BS (°)	E-BS (°)
Non-covering	527	230	7.3	76.9	72.0	1.00	−2.0
Covering	644	375	7.0	75.6	75.0	−10.0	9.0

The effect of the circle slot diameter towards the RL and the AR of the antenna is plotted in Fig. 5(d). The dimension of the circle slot has not significantly affected the AR performance, but in turn, it has changed the RL characteristic of the antenna. The IBW and ARBW are also not affected by changing the circular slot diameter. Also, the circle slot does not affect significantly either the resonant frequency response or the surface current distribution direction of the parasitic patch. Estimated length for diameter r_o is arranged between value of $w_p = 22.46$ mm and $w_p = 26.95$ mm (20% of w_p). After optimization, the optimum IBW and ARBW of the propose antenna are obtained with value of r_o equal to 26.5 mm (17.98% of w_p).

3. ANTENNA PROTOTYPE AND PERFORMANCE VERIFICATION

Figure 6 depicts the fabricated antenna in its separate substrate, the top substrate with the parasitic patch and the bottom substrate with the radiating patch. The substrates are then stacked and fixed

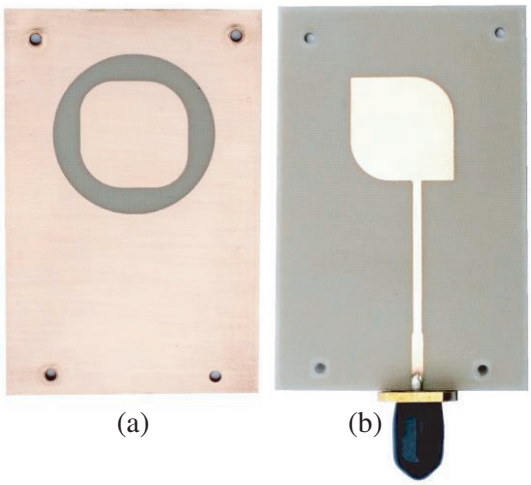

Figure 6. Prototype of the antenna: (a) top substrate; (b) bottom substrate.

together in their position by using 2 mm plastic screws at every corner of the antenna. Female 50 Ω SMA connector was soldered to the end of the feed line as the in or out port of the antenna. The fabricated antenna has a total dimension of 42.4 mm in width, 65.5 mm in length, and 3.3 mm in thickness.

The performance of the antenna is measured in an anechoic chamber using E8364C PNA Microwave Network Analyzer. Fig. 7 shows the measured performance of the antenna as compared to its simulated characteristics. The simulated and measured RLs are illustrated in Fig. 7(a). The desired operational

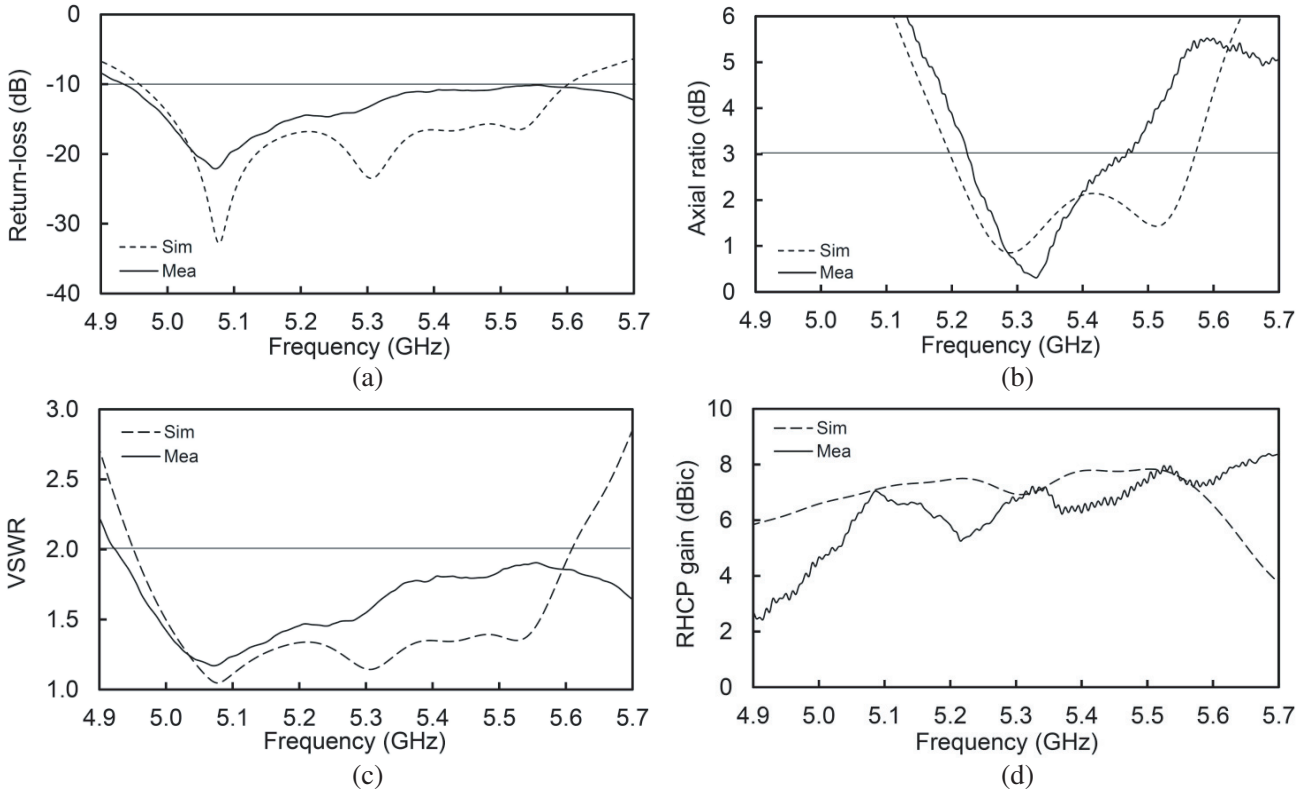

Figure 7. Simulated and measured performance of the antenna. (a) return loss; (b) axial ratio; (c) VSWR; (d) gain.

Table 4. A summary of similar antennas in literature. Note: size is expressed by width × length × thickness.

Antenna	Structure	Feeding type	f_c (GHz)	IBW (%)	ARBW (%)	Gain (dBic)	Dimension (mm)
Ref. [26]	Stacked; air gap	Pin	6.00	31.5	20.7	8.6	40 × 40 × 4.5
Ref. [27]	Single; parasitics	Pin	5.50	19.5	12.9	9.8	50 × 50 × 1.5
Ref. [28]	Single; slot ,	Line	5.50	34.5	14.5	3.6	25 × 25 × 0.8
Ref. [29]	Stacked; air gap ,	Line	6.00	60.0	56.0	4.4	40 × 40 × 6.5
Ref. [30]	Single; slot	Line	5.75	90.2	40.0	4.5	25 × 25 × 1.6
Proposed	Stacked; parasitic	Line	5.30	20.9	4.7	7.1	42 × 65 × 3.2

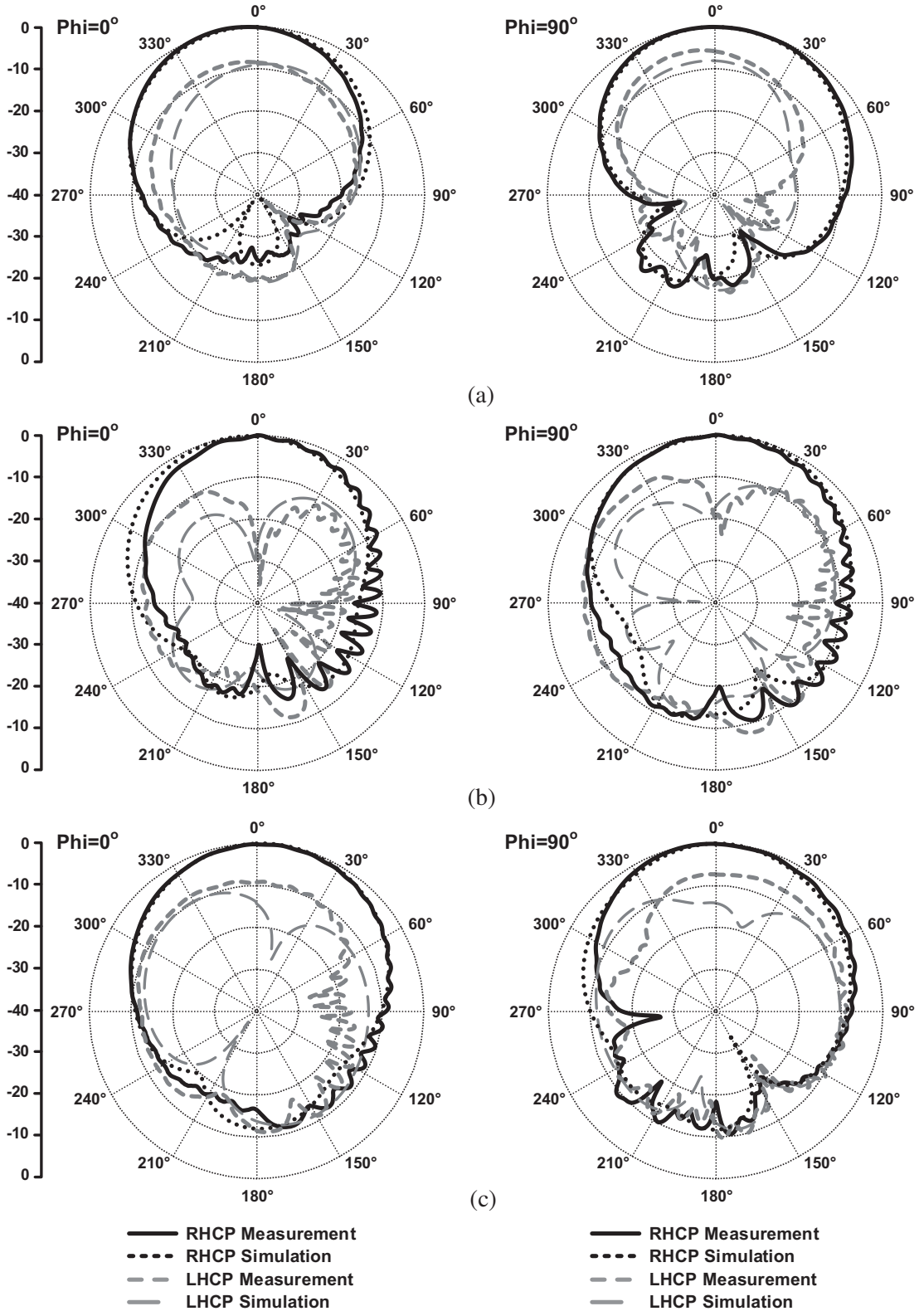

Figure 8. Simulated and measured radiation pattern in H-plane (phi = 0°) and E-plane (phi = 90°) at frequency of: (a) 5.1 GHz; (b) 5.3 GHz; (c) 5.5 GHz.

bandwidth of the airborne CP-SAR array antenna system is shown by the shadowed-bar in the frequency axis. From the graph, it is clearly shown that the RL of proposed antenna has fulfilled the requirements. The simulated and measured IBWs are approximately 640 MHz (spanning from 4.96 GHz to 5.6 GHz) and 1,110 MHz (spanning from 4.94 GHz to 6.04 GHz), respectively. Fig. 7(b) shows the simulated and measured ARBWs. From the graph, the ARBW bandwidths are approximately 380 MHz (spanning from 5.20 GHz to 5.58 GHz) and 250 MHz (spanning 5.23 GHz to 5.48 GHz). The measured ARBW still needs to be improved to fulfill the required specification. It will be significantly improved in the next phase where an array of the patches will be designed using serial sequential rotation technique. The characteristic of voltage standing wave ratio (VSWR) is verified and presented in Fig. 7(c), where simulated and measured values indicate good performance within operating bandwidth with the value of less than 2. The VSWR at the center frequency (5.3 GHz) is less than 1.5. Fig. 7(d) compares the simulated and measured gains of the antenna. They exhibit similar trends at the operational bandwidth from 5.1 GHz to 5.5 GHz. At the center frequency, the gain was recorded to be 7 dBic. Some of the measured results were not in accordance with the simulations, and they can be attributed to possible fabrication errors, such as multiple dissimilarities on printed microwave stacked substrate structure (stripline) that consists partly of dielectric material and partly of air, misalignment between top substrate and bottom substrate, or under-etching process. Also additional reflections of the connector, cable attenuation, and phase shift of the measurement instruments are unavoidable effects in mismatching the simulated and realized antenna.

Table 4 summarizes the performance of the realized antenna in comparison to other similar antennas in the literature, to illustrate the effect of the antenna structure and feeding type towards the antenna performance. The table shows that antennas with microstrip line feeding could reach wider IBW and ARBW than pin-fed type antennas. Regarding the gain, antennas with pin-fed and parasitic patch exhibit better performance. Also, the antennas with broad IBW can be built by using stacked substrates or by applying a slotted shape on the parasitic patch. The proposed antenna has the highest gain among the antennas with microstrip line feeding.

Figure 8 shows the simulated and measured radiation patterns of the prototype in the H-plane and E-plane in several frequencies. The normalized radiation pattern for each frequency is plotted in one plot, for both co-polarization and cross-polarization. At all frequencies, the main lobe direction is not exactly centered at 0° in both H-plane and E-plane. The main lobe direction of the prototype at frequency 5.3 GHz is at −3° in H-plane and at 9° in E-plane. This is caused by shifting the line feed position in the radiating patch to increase the ARBW of the antenna. At frequencies of 5.1 GHz and 5.5 GHz, the cross-polarization level is less than −20 dB, and at frequency of 5.3 GHz the cross-polarization levels reach around −20 dB in both planes.

4. CONCLUSIONS

A single antenna wide bandwidth CP microstrip antenna for C-band airborne CP-SAR remote sensing application was designed, manufactured, and measured. A wide IBW was achieved by using a thick substrate with low dielectric constant, double-stacked substrate structure, modified shape of radiating patch and circle slotted parasitic patch. The measurement results show that the IBW of the antenna is 1,110 MHz (20.87%) and hence, fulfills the required specification. The measured ARBW for the prototype is 250 MHz (4.72%) and still needs improvement to fulfill the required specification. The gain of the antenna is improved to 7 dBic by parasitic patch to the top layer of the antenna. It is also found that the IBW and ARBW were improved by adding a circle slotted and top copper-covering to the antenna. In future work, this single patch antenna design will be arranged in 8×8 and 8×16 elements of an array configuration in order to achieve a total gain of more than 20 dBic. Also in order to get a wider ARBW, fully serial sequential rotation techniques on the feeding network will be implemented.

REFERENCES

1. Sri Sumantyo, J. T., K. V. Chet, L. T. Sze, T. Kawai, T. Ebinuma, Y. Izumi, M. Z. Baharuddin, S. Gao, and K. Ito, "Development of circular polarized synthetic aperture radar onboard UAV JX-1," *International Journal of Remote Sensing*, Vol. 38, Nos. 8–10, 2745–2756, 2017.

2. Ouchi, K., "Recent trend and advance of synthetic aperture radar with selected topics," *Remote Sensing*, Vol. 5, No. 2, 716–807, 2013.
3. Gail, W. B., "Effect of faraday rotation on polarimetric SAR," *IEEE Int. Transactions on Aerospace and Electronic System*, Vol. 34, No. 1, 301–307, 1998.
4. Gao, S., Q. Luo, and F. Zhu, *Circularly Polarized Antenna*, John Willey Sons, 2014.
5. Balanis, C. A., *Antenna Theory Analysis and Design*, 3rd Edition, A John Willey and Sons, New Jersey, 2005.
6. James, J. R. and P. S. Hall, *Handbook of Microstrip Antennas*, Peter Peregrinus Ltd, London, UK, 1989.
7. Stutzman, W. L. and G. A. Thiele, *Antenna Theory and Design*, 2nd Edition, John Wiley and Sons, 1998.
8. Carver, K. R. and J. W. Mink, "Microstrip antenna technology," *IEEE Transactions on Antennas and Propagation*, Vol. 29, No. 1, 2–24, 1981.
9. Hung, K. F. and Y. C. Lin, "Novel broadband circularly polarized cavity-backed aperture antenna with traveling wave excitation," *IEEE Transactions on Antenna and Propagation*, Vol. 58, No. 1, 35–42, 2009.
10. Davidson, K., Y. Antar, and A. Freundorfer, "A wideband via fed circularly polarized microstrip antenna on a multi-layer substrate," *IEEE Antennas and Propagation Society International Symposium, APS-URSI 2013*, Vol. 9, No. 6, 1468–1469, 2013.
11. Singh, D. K., B. K. Kanaujia, S. Dwari, G. P. Pandey, and S. Kumar, "Multiband circularly polarized stacked microstrip antenna," *Progress In Electromagnetic Research C*, Vol. 56, 55–65, 2015.
12. Lai, H. W., D. Xue, H. Wong, K. K. So, and X. Y. Zhang, "Broadband circularly polarized patch antenna arrays with multiple layers structure," *IEEE Antenna and Wireless Propagation Letters*, Vol. 16, 525–528, 2017.
13. Pozar, D. M. and B. Kaufman, "Increasing the bandwidth of a microstrip antenna by proximity coupling," *Electronics Letters*, Vol. 23, No. 8, 368–369, 2007.
14. Sharma, P. C. and K. C. Gupta, "Analysis and optimized design of single feed circularly polarized microstrip antennas," *IEEE Transactions on Antenna and Propagation*, Vol. 31, No. 6, 949–955, 1983.
15. Chung, K. L. and A. S. Mohan, "A systematic design method to obtain broadband characteristics for singly-fed electromagnetically coupled patch antennas for circularly polarization," *IEEE Transactions on Antenna and Propagation*, Vol. 51, No. 12, 3239–3248, 2003.
16. Wu, J., X. Ren, Z. Wang, and Y. Yin, "Broadband circularly polarized antenna with L-shaped strip feeding and shorting-pin loading," *IEEE Antenna and Wireless Propagation Letters*, Vol. 13, 1733–1736, 2015.
17. Targonski, S. D. and M. Pozar, "Design of wideband circularly polarized aperture-coupled microstrip antennas," *IEEE Transactions on Antenna and Propagation*, Vol. 41, No. 2, 214–220, 1993.
18. Sze, J. Y. and W. H. Chen, "Axial ratio bandwidth enhancement of a microstrip-line-fed circularly polarized annular-ring slot antenna," *IEEE Transactions on Antenna and Propagation*, Vol. 59, No. 7, 2450–2456, 2011.
19. Saini, R. K. and S. Dwari, "A broadband dual circularly polarized square slot antenna," *IEEE Transactions on Antenna and Propagation*, Vol. 64, No. 1, 290–294, 2015.
20. Gyasi, K. O., G. Wen, Y. Huang, E. Affum, and W. Hu, "Broadband circularly polarized cross shaped slot antenna with an improved feedline," *Progress In Electromagnetics Research C*, Vol. 74, 141–149, 2017.
21. Ding, K., C. Gao, T. Yu, D. Qu, and B. Zhang, "Gain-improved broadband circularly polarized antenna array with parasitic patches," *IEEE Antenna and Wireless Propagation Letters*, Vol. 16, 1468–1471, Dec. 2016.

22. Fu, S., Q. Kong, S. Fang, and Z. Wang, "Broadband circularly polarized microstrip antenna with coplanar parasitic ring slot patch for L-band satellite system application," *IEEE Antenna and Wireless Propagation Letters*, Vol. 13, No. 1, 943–946, 2014.
23. Sung, Y., "Bandwidth enhancement of a microstrip line-fed printed wide-slot antenna with parasitic center patch," *IEEE Transactions on Antenna and Propagation*, Vol. 60, No. 4, 1712–1716, 2012.
24. Yohandri, V. W., I. Firmansyah, P. Rizki Akbar, J. T. Sri Sumantyo, and H. Kuze, "Development of circularly polarized array antenna for synthetic aperture radar broadband sensor installed on UAV," *Progess In Electromagnetics Research C*, Vol. 19, 119–133, 2011.
25. Baharuddin, M. Z. and J. T. S. Sumantyo, "Suppressed side-lobe, beam steered, C-band circularly polarized array antenna for airborne synthetic aperture radar," *The Journal of Unmanned System Technology*, Vol. 4, No. 1, 2016.
26. Yang, W., J. Zhou, Z. Yu, and L. Li, "Single-fed low profile broadband circularly polarized stacked patch antenna," *IEEE Transactions on Antenna and Propagation*, Vol. 62, No. 10, 5406–5410, 2014.
27. Ding, K., C. Gao, D. Qu, and Q. Yin, "Compact broadband circularly polarized antenna with parasitic patches," *IEEE Transactions on Antenna and Propagation*, Vol. 65, 2017.
28. Rafii, V., J. Nourinia, C. Ghobadi, J. Pourahmadazar, and B. S. Virdee, "Broadband circularly polarized slot antenna array using sequential rotated technique for C-band application," *IEEE Antenna and Propagation Letters*, Vol. 12, No. 1921, 128–131, 2013.
29. Ellis, M. S., Z. Zhao, J. Wu, X. Ding, Z. Nie, and Q. H. Lin, "A novel simple and compact microstrip-fed circularly polarized wide slot antenna with wide axial ratio bandwidth for C-band application," *IEEE Transactions on Antenna and Propagation*, Vol. 64, No. 4, 1552–1555, 2016.
30. Zhang, H., Y. C. Jiao, L. Lu, and C. Zhang, "Broadband circularly polarized square-ring-loaded slot antenna with flat gains," *IEEE Antenna and Wireless Propagation Letters*, Vol. 16, No. 99, 29–32, 2017.